Article

The Implementation of AFM-Based Nanoscale Diagnostic Methods in the Investigation of the Degradation Process of Bacteriostatic Acrylic Film with Silver Nanoparticles

Andrzej Sikora [1,*] and Łukasz Witos [2]

[1] Department of Nanometrology, Faculty of Electronics, Photonics and Microsystems, Wrocław University of Science and Technology, 11/17 Janiszewskiego St., 50-372 Wroclaw, Poland
[2] Kendromed, Sołtysowicka 25 A, 51-168 Wrocław, Poland; witos.l@kendromed.pl
* Correspondence: andrzej.sikora@pwr.edu.pl

Featured Application: Thin polymer film durability and resistance to certain exposure tests.

Abstract: In this paper, a custom-tailored investigation protocol aimed at the tests of the resistance of bacteriostatic acrylic-based film containing silver nanoparticles is presented. As hospital appliance applications were considered, it was necessary to provide a unique approach, enabling specific media exposure and utilizing high-sensitivity measurement methods to observe fine indications of material wear. Due to the presence of nanoparticles in the tested film, nanometer-resolution surface imaging is necessary. Therefore, the main source of information about its degradation process is atomic force microscopy (AFM) measurements. This particular tool is an appreciated source of information, providing quantitative data about both morphological and mechanical changes in the properties of the surface. Using such an approach, supported by standard diagnostic methods, such as colorimetry and wettability angle determination, it was possible to enable insights into the way the bacteriostatic film deteriorates and evaluate its usefulness in medical appliance applications. Further tests of various films developed by companies can be performed using the described protocol to determine the lifetime of certain products. This paper reveals the company's practical utilization of both standardized and novel test techniques in the evaluation of new products.

Keywords: nanomaterials; atomic force microscopy; acrylic film; bacteriostatic layer; colorimetry; wettability; roughness; mechanical properties

1. Introduction

One of the major challenges in clinical practice is the need for the reduction of hospital-acquired infections (HAIs). The total amount of annually diagnosed HAI cases in the USA is 1.8 million cases, where, for almost 100,000 patients, the infection is lethal. It should be underlined that breast cancer, AIDS, and car accidents together take fewer lives annually than HAIs [1]. Therefore, the scale of this problem encourages various agencies and companies to develop solutions, providing a significant reduction of this issue.

Recently performed studies showed that the issue of HAIs is one of the most important causes of extended hospitalization due to additional therapy or even deaths [2–6]. As it is identified in a significant fraction of patients (even more than 30%), it is addressed using various approaches. While analyzing the surveys, one can point out the most often identified pathogens, *Staphylococcus aureus*, *Escherichia coli*, *Klebsiella pneumoniae*, and *Pseudomonas aeruginosa*; however, this list changes when one focuses on certain medical procedures and the patient's age. It should be underlined that the presence of antimicrobial resistance (AMR) requires the application of new-generation drugs, yet at some point, no therapy is effective. Therefore, the means to reduce infection risk must be taken. As studies have proven, no patient contact is necessary to contaminate hospital staff with the bacteria

in the room; hence, all possible pathogen transmission paths must be cut at every level. Thus, it becomes clear that an essential role of infection reduction may be the equipment if bacteriostatic properties of the surface are implemented.

Progress in hospital equipment development is enabled by the introduction of technical solutions providing new or improved functionalities. Also, better safety features are available, particularly in reducing the bacteria survival ratio. As the companies aim to meet the needs of the market, various solutions are tested in order to verify the potential usefulness of various substances to obtain a bacteriostatic film over the equipment's surface. One promising solution is nano-silver (silver nanoparticles—Ag NPs)-based antibacterial solutions [7–12]. In particular, polymer-based coatings containing nanoparticles may be a very useful approach [13].

The acrylic-based paint containing silver nanoparticles was one of the first selections. The bacteriological tests using *Escherichia coli* ATCC25922 (according to ISO 22196:2007 standard [14]) showed satisfying efficacy of the investigated film in terms of bacteriostatic properties, with an R value of 5.30 log (78.3%). Also, the results of the preliminary test were promising, while the obtained coverings of the equipment made of aluminum revealed satisfying adhesion and homogeneity. However, the reliability verification of the surface is one of the major issues that the producer has to evaluate. The expected lifetime of such products must be not less than 5 years. As the unique environment is considered in terms of the conditions that the material has to show resistance to, application-tailored test procedures providing insight into the degradation process of the bacteriostatic film have to be developed.

In order to perform time-accelerated tests of the developed coating, a customer-tailored protocol was developed, as standard protocols appeared to be insufficient in terms of nanoparticle-based thin film coverings. In principle, the conditions typical for hospitals had to be taken into account, so adequate exposure and degradation methods were chosen. One has to be aware that the test methods of the deterioration of films made of nanomaterials must be adequate for the investigated object and phenomena. Therefore, some standard-defined test solutions are not sufficient in terms of the required outcome. The list of both the exposure method and the test techniques is given in the following chapter. The developed test approach, with particular emphasis on verification methods based on high-sensitivity techniques, such as atomic force microscopy, is a considerable advantage due to its diagnostic potential. It solves a critical issue of obtaining reliable and quantitative data about the deterioration ratio of a certain product in terms of application at specific conditions, where high sensitivity over a relatively short test period with small dimensions of the specimens, such as thin films, are the key advantages. Additionally, AFM is one of the fine nanoscale diagnostic tools that does not require complex preparation of the investigated sample, while in the case of SEM (scanning electron microscopy), dielectric samples should be covered with a thin conductive film, which is considered at some degree as the surface's roughness alteration.

Therefore, the present approach can be desired by a number of entities active in the field of the development and fabrication of a variety of films and coverings, where the evaluation of the wear and degradation of the films is essential, and no macroscopic method may provide reliable data, in particular, at early aging stages. The market related to such products can be estimated to be hundreds of thousands of dollars annually at the moment. It should be emphasized that the unique detection sensitivity of atomic force microscopy, providing complex information about changes in the material's properties with ultimate resolution, enables the degradation tests in short periods, which is particularly important for the industry. Moreover, this particular technique allows us to test the specimens, which, due to their small dimensions, can not be investigated with other methods. Therefore, the potential value of the method increases with a reduction in the size of the object under test, as well as the available test time.

2. Materials and Methods

Typical aluminum profiles used for medical equipment fabrication were utilized in the tests. The construction aluminum 6000 series profiles were fabricated using extrusion method with an aluminum smelter, according to technical specifications provided by the equipment manufacturer.

The film was fabricated by spray painting according to the specifications of the paint delivered by the third party. Once the surface was dry, the samples were tested. Three sets of samples were prepared: A—reference sample, B—sample exposed to a single dose, C—sample exposed to a double dose. A view of the product with new film, as well as photography of a small part of the element utilized in the tests, are shown in Figure 1.

(**a**) (**b**)

Figure 1. View of the product with new coating (**a**). Close-up photography of the surface with coating used for tests (**b**).

2.1. The Exposure Parameters

The exposures were adjusted in order to simulate the conditions one can expect in hospital conditions, taking into account solar and UV radiation used for disinfection, including increased temperature and humidity, as well as presence of chemicals used for cleaning medical equipment surfaces. Those factors are the most significant in terms of polymer deterioration.

The single-dose exposure parameters to a certain set of media were as follows:

- Simulated solar radiation [15] (Xenon lamp)—100 h (details are shown in Table 1);
- UV radiation typically utilized for the air and room sterilization—500 h (details are shown in Table 2);
- Increased humidity (RH 98%) and temperature (40 °C)—72 h;
- Increased temperature (70 °C)—48 h;
- Chemical disinfection substances typically utilized in medical units, 24 h exposure for each substance:

    ○ Incidin Liquid Spray;
    ○ Lysoformin Plus Schaum;
    ○ Aldewir (10% solution).

For doubled doses, all the time periods given above were multiplied by two. It has to be underlined that the spraying causes thermal shock on the surface; therefore, it mimics a much harsher environment than in the case of exposure without spraying.

The following test methods were utilized to observe the degradation of the developed films:

- The roughness measurements by means of atomic force microscopy (AFM) provided insight into the deterioration of the material by quantitative tracing of the morphological changes of the surface [16–23].

- The mechanical property measurements from atomic force microscopy enabled the detection of the degradation of the outer layers of the material in terms of changes in stiffness and adhesion [23–25].
- Wettability tests provided complementary information to the roughness measurement concerning the practical aspects of the utilization of the film in particular conditions [25].
- Colorimetric analysis gave information concerning the loss of aesthetical aspects of the film as well as phenomena responsible for the aging process [26].

Table 1. The simulated solar radiation exposure parameters.

Device	Atlas Ci65
Basic exposure time	100 h
Type of the lamp	Xenon
Spraying of the samples	102 min (no spraying) 18 min (spraying)
Black plate's temperature	65.1 °C (during dry periods)
Dry thermometer temperature	47.0 °C (average value during the dry periods)
Relative humidity during the exposure	48% (average value during the dry periods)
The radiation intensity of full spectra of the xenon lamp (290 nm < λ < 800 nm)	$374 \frac{W}{m^2}$
The radiation intensity of UV spectra of the xenon lamp (290 nm < λ < 800 nm)	$41.14 \frac{W}{m^2}$
The radiation intensity of the xenon lamp λ = 340 nm	$0.34 \frac{W}{m^2 \cdot nm}$

Table 2. The UV light exposure parameters.

Basic Exposure Time	500 h
Type of lamp	evanescent
Spraying of the samples	no spraying
Black plate's temperature	37.1 °C
Relative humidity during the exposure	48% (average value during the dry periods)
The radiation intensity of the evanescent lamp λ = 253 nm	$9 \frac{W}{m^2}$

2.2. AFM Measurements

AFM measurements were performed with DI3000 system (Digital Instruments, Santa Barbara, CA, USA) equipped with 100×100 μm X-Y scanner. Topography imaging was carried out in TappingMode using standard probes (Nanosensors Pointprobes: nominal tip radius $r_{tip} = 10$ nm, resonance frequency $f_{res} = 306$–353 kHz, and spring constant range $k = 43$–68 N·m^{-1}) under ambient conditions. The scanning area was 3×3 μm; typical scanning speed was approx. 1 μm/s. The set of three topography data points was acquired for each sample in order to provide statistically significant data, as local morphological non-homogeneities could be noticed and excluded. The roughness values distribution allowed us to assume that the acquired data could be utilized for further analysis, providing expected consistency. In addition, 50×50 μm images were also acquired to confirm the homogeneity of the surface on a larger scale. The 3×3 μm scanning area allowed us to observe the presence of silver nanoparticles in the polymer film; therefore, the data obtained for this area was utilized in further analyses, while the nanoscale appearance of

surface degradation can be noticed in the area of matrix-filler interphase. Images at both scales are shown in Figure 2.
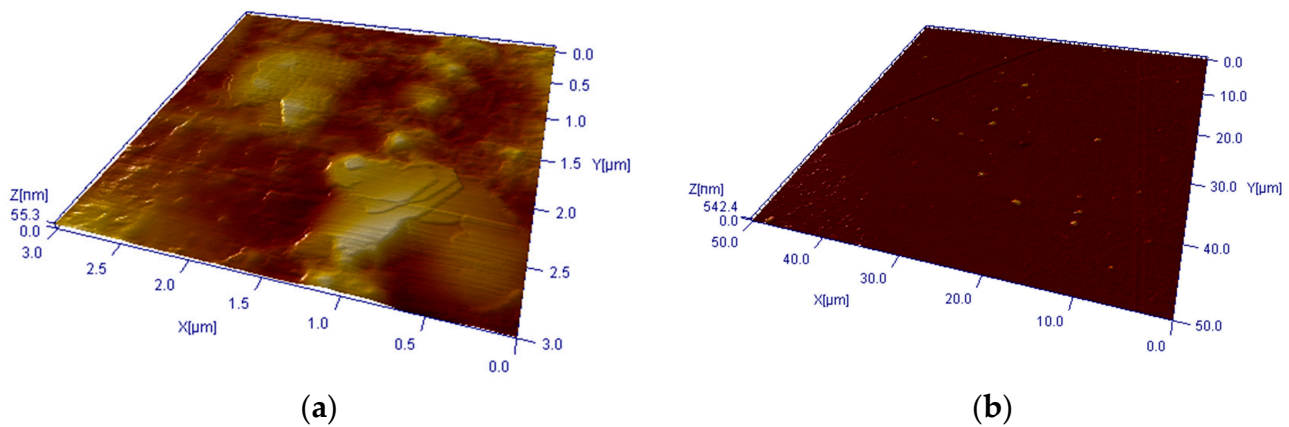

Figure 2. Examples of 3D views of surface topography of investigated samples. (**a**) Sample at 3×3 μm scan size. (**b**) Sample at 50×50 μm scan size.

The mechanical properties of the film were determined using force spectroscopy, where contact probes NTMDT CSG30 (0.6 N·m^{-1}, 6 nm radius) were used. In order to provide required measurement accuracy, the reference sample was utilized [27,28]. Approach/retract speed was 10 nm/s. The maximum tip-sample force was limited to 75 nN in order to avoid sample's deformation and tip damage. The measurements were performed using following procedure: the force–distance acquisition was performed 10 times in a single spot; then, the probe's location was changed, and the acquisition procedure was repeated within an area of 3×3 μm. This process was continued while nine sets of curves were acquired. Then, in order to avoid the influence of local non-homogeneities, the measurement spot was changed three times, where the whole data collection procedure was performed.

The topography data was processed using SPIP software (version 5.1.7) from Image Metrology [29], and force spectroscopy curves were analyzed while the DMT model was utilized. In both cases, median value was calculated and used in the analysis, and standard deviation was used to evaluate the uniformity and repeatability of the calculated values. Example of the force–distance curve is shown in Figure 3.
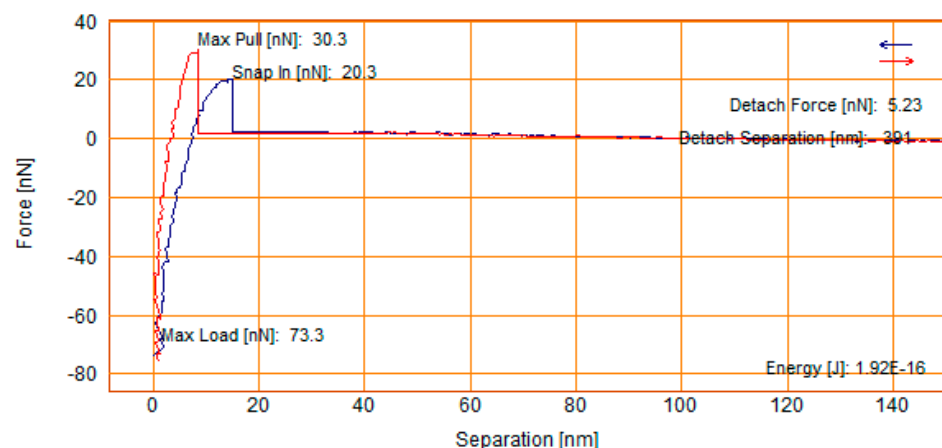

Figure 3. Example of the force–distance curve.

2.3. Wettability Determination

The wettability was determined using semi-automatic home-made system. The mechanized liquid dosing system allowed application of repeatable amounts of water on the surface at a given height. The computer equipped with a microscopic camera acquired images of droplets as a movie; therefore, one could determine wettability angles considering time as a parameter. The contact angle was determined using vector-based analysis software, enabling the measurement resolution below 0.1 deg. For each sample, at least five measurement values were obtained at different locations on the surface to provide a statistical approach. An example of the acquired image is shown in Figure 4.
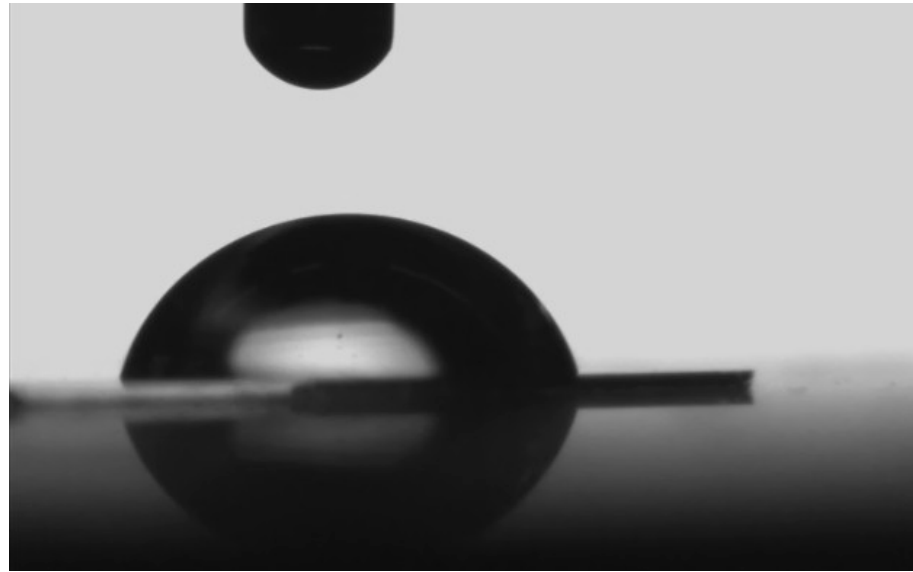

Figure 4. Example of the images acquired with microscope camera during wettability angle determination.

2.4. Colorimetric Analysis

The discoloration of the investigated samples was measured using a home-made system containing computer equipped with CCD camera, providing 4 Mpix resolution in an area range 50×50 mm. The measurement chamber eliminated the external light influence, while internal LED-based lighting system obtained repeatable, stable illumination. In order to verify the measurement quality, the test grid was used before each test.

In order to obtain L*a*b colorimetric system data, the RGB components were extracted using statistical analysis of generated files and compared, taking into account other acquired data. The examples of collected images are shown in Figure 5.
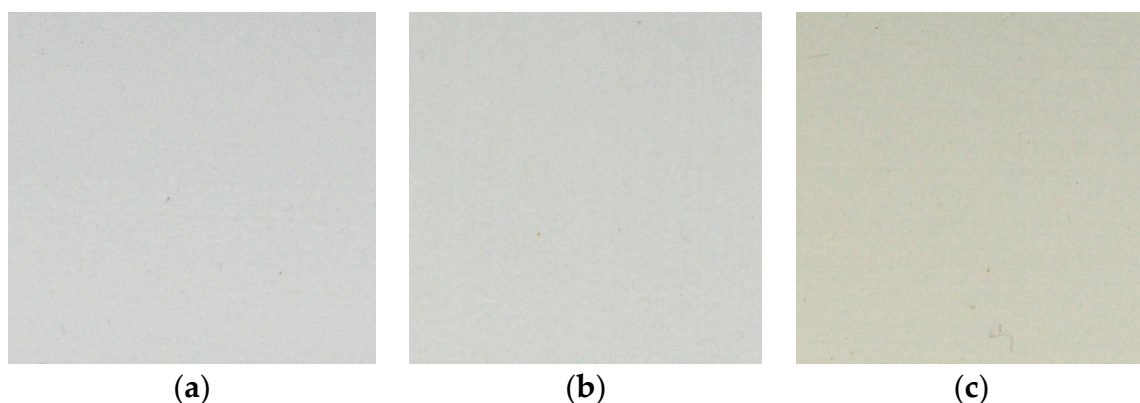

(a)   (b)   (c)

Figure 5. Examples of the colorimetry tests. Samples (**a**–**c**) from left to right.

3. Experimental Results

The acquisition of the topography maps using atomic force microscopy allowed us to observe significant morphological changes due to exposure to the set of previous conditions (Figure 6). While the reference surface was relatively flat, with no discontinuities, and the presence of large (up to 1 μm in diameter) silver particles could be noticed, sample B reveals the first signs of degradation, such as cracks and pinholes. On the other hand, in the case of sample C, a vast reduction in the volume of the material is visible, showing advanced degradation of the acrylic matrix.
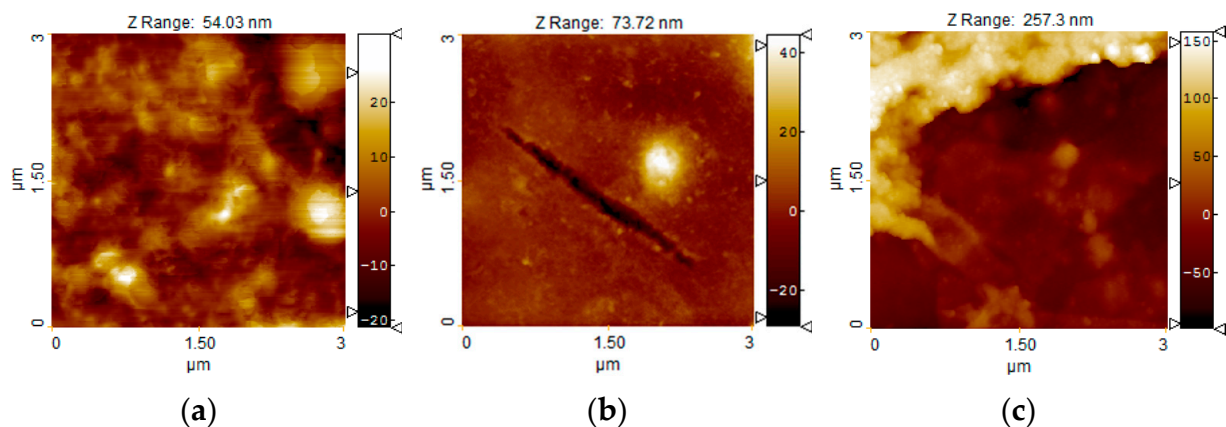

Figure 6. Examples of the topography images acquired using atomic force microscopy (AFM). Samples (**a**–**c**) from left to right.

In order to compare the morphological changes in a quantitative fashion, the roughness parameters were calculated. The acquisition of several sets of data for each sample allowed us to calculate the average value and the distribution of the parameters, providing insights into the homogeneity of the surfaces. The following parameters are shown in Figure 7 (Supplementary Materials Figure S1): average roughness (S_a), root mean square roughness (S_q), peak–peak value (S_z), and the surface area ratio (S_{dr}). A significant increase in all of the presented parameters is clearly visible. A rapid increase in S_z is related to the appearance of the first cracks and pinholes penetrating the volume of the film. The vertical bars show the standard deviation within the set of measurement data. A further increase in this parameter has smaller dynamics as the process switches to the volume loss. It should be noted that the standard deviation bars reveal that the spatial non-homogeneities of the surface are smaller than observed roughness changes. This important information allows us to claim that the measurements are meaningful and can be used for the analysis. Additionally, the exceptionally large SD bar in S_z for the second sample shows that at a certain point of deterioration, quite large cracks appear in the surface (visible in Figure 6), which initiate the mechanical degradation of the surface.

One of the advantages of the AFM method is the measurement of the mechanical properties of the surface. Figure 8 (Supplementary Materials Figure S2) shows the changes in stiffness and adhesion measured using the force spectroscopy technique. The stiffness increase, along with the adhesion reduction, revealed the tendency of the film to peel off after the doubled exposure. This phenomenon was also confirmed by the macroscopic observation. Further analysis revealed that UV exposure causes further polymer networking, hence hardening.
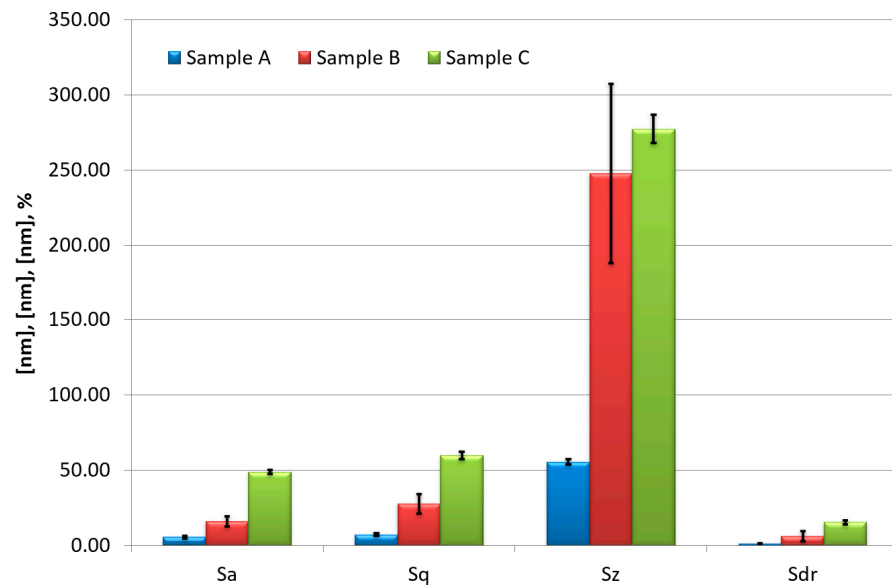
Figure 7. The roughness parameter comparison for investigated samples.
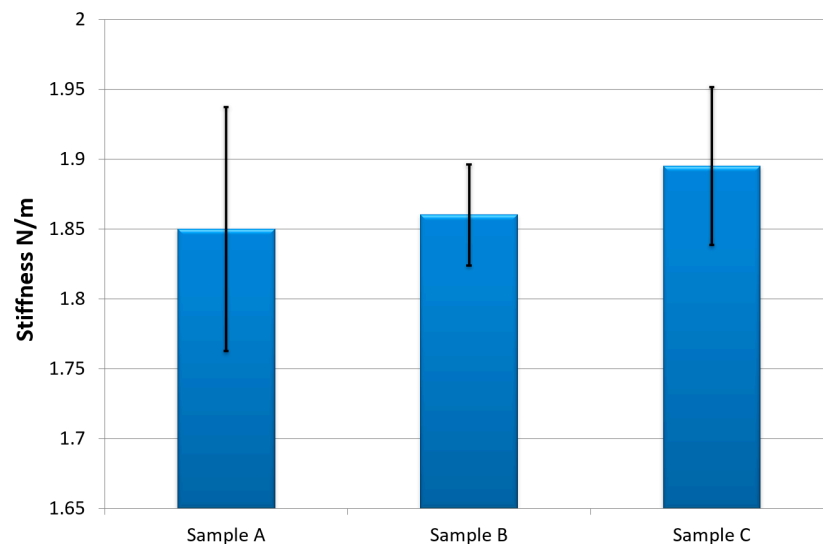

Figure 8. The comparison of stiffness changes for investigated samples.

While the durability of the surface is one of the most desired properties, some elasticity is also necessary to avoid the presence of too much tension between the substrate and the film. Therefore, one can expect a complete dysfunction of the film once similar conditions are present in real applications. Such a conclusion can be considered as the basis of the disqualification of the investigated film. This stage of the experiment allowed us to notice the expected lifetime of the antibacterial film. The exploitation period causing the exposure conditions simulated for sample B could be acceptable, but the double-time use would cause damage to the film. On the other hand, the pull force (visible also in Figure 3), which reveals the adhesion force present between the surface and the scanning tip, decreased while exposure was applied (Figure 9). (Supplementary Materials Figure S3). The observed behavior may indicate a reduced ability of the film to stick to other surfaces, which, in connection with other processes, can cause the film to detach from the substrate [30].
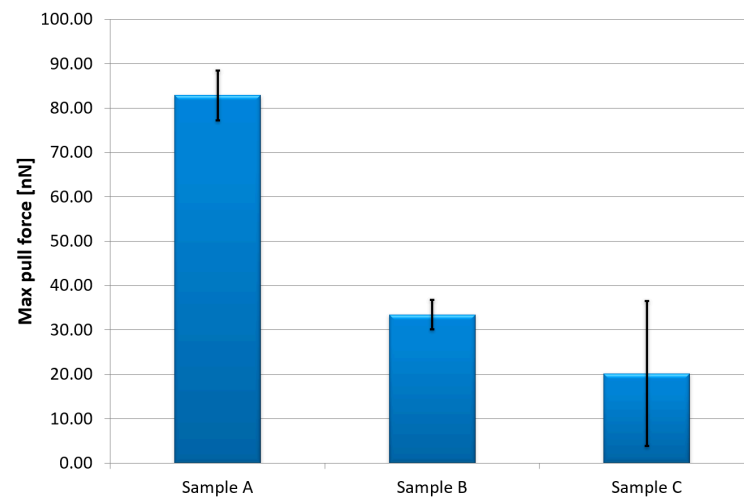
Figure 9. The comparison of maximum pull force for investigated samples.

The wettability measurements showed a significant decrease in the contact angle (Figure 10). (Supplementary Materials Figure S4). The changes are coherent with the roughness parameters; however, the dynamics of the process differed for both test methods. Such a phenomenon indicates a possible worsening of the surface's cleaning, which has a major impact on safety in hospitals. In addition, one must also take into account the influence of the degradation process on the bacteria's nesting ability on the surface. This issue may play a certain role in the decrease of the bacteriostatic efficacy of the material. It should be underlined that as AFM measurements may provide the majority of essential data for determining the product's aging ratio, this particular diagnostic technology reaches its maturity while appropriate measurement protocols and data processing data are developed and tested [31–35]. The usefulness of this approach and its complementary value to other methods used in this work is continuously tested and proven.
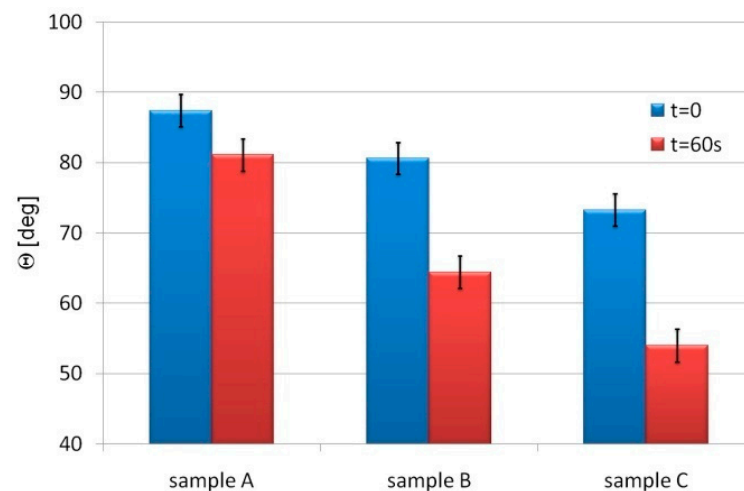

Figure 10. The wettability changes of the film surface for tested samples.

The colorimetric analysis (according to CIELAB color space) [36] revealed a decrease in the luminance (*L* value) along with a change in the color component parameters (Figure 11): *a* – (red/green axis value) the decrease shows a shift to green color, and *b* – (yellow/ blue axis value) the increase shows a shift to yellow color. The arrows shown in Figure 11 (Supplementary Materials Figure S5) present the shift of certain components values, while the vertical bars show the standard deviation of values obtained from whole digital image of investigated sample. The obtained data show the major cause of the material's degradation, which is photo-oxidation. One could take into account the aesthetic issue, as the film is

planned to be used in equipment for everyday use. It has to be emphasized that below a certain thickness, the film can not be investigated using the colorimetric analysis, as the distances between the material–photon interactions are insufficient. Again, coherently to the AFM measurements, the analysis showed that the changes in the film properties after aging with dose B can still be acceptable (the color change was close to distinction), while for dose C, the discoloration is significant.
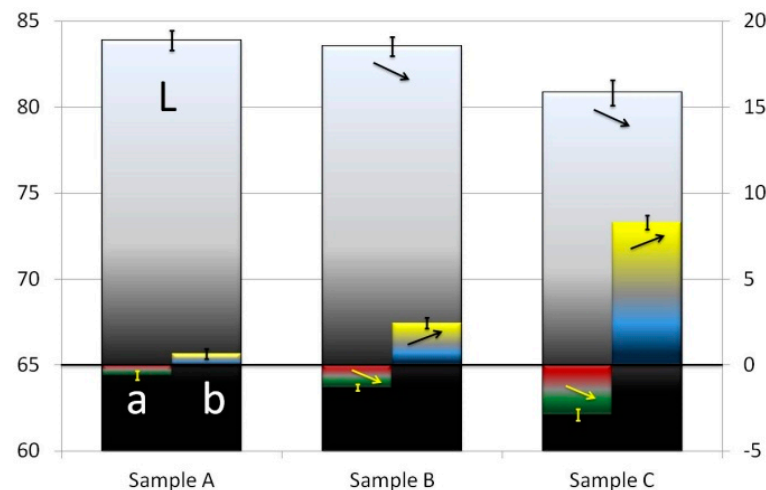

Figure 11. The results of colorimetric analysis of the degradation of the samples.

The antibacterial activity of Ag NP films was investigated in a specialized biological laboratory, according to the ISO 22196:2007 standard [14]. The bacteriological test using *Escherichia coli* ATCC25922 was performed. Two samples were delivered: the aluminum profiles covered with acrylic-based film containing the silver nanoparticles and acrylic-based film without Ag NPs (control sample). On both surfaces, 0.4 mL of fluid containing microorganisms was placed. Then, samples were stored in a humid environment. In order to determine the amount of bacteria, the inoculum was washed from the tested surfaces and incubated using TSA agar. The incubation lasted 24 h at 37 °C. The amount of living *Escherichia coli* bacteria in the inoculum was 1.2×10^6 jtk/mL. The test results are shown in Table 3.

Table 3. The antibacterial activity test results.

The Results Obtained for Test and Control Sample								
Determined Parameter	**Tested Sample Directly at Start Moment**			**Control Sample after 24 h**			**Tested Sample after 24 h**		
Amount of living cells on sample	9.9×10^3	1.0×10^4	9.2×10^3	7.2×10^6	6.0×10^6	4.3×10^6	3.8×10^1	1.3×10^1	3.8×10^1
Average	9.8×10^3			$5.8 \times 10^6 \Rightarrow 6.77$ log			$2.9 \times 10^1 \Rightarrow 1.46$ log		

The results revealed satisfying efficacy of the investigated film in terms of bacteriostatic properties, while the R parameter was 5.30 log (78.3%).

4. Discussion and Conclusions

This paper presents the results of the development and utilization of the unique test protocol designed to investigate the deterioration process of bacteriostatic films. The tests were performed according to the customer-tailored protocol, developed in cooperation with the equipment producer and were aimed at the verification of the resistance of the acrylic-based films containing silver nanoparticles to the conditions typical for the hospital environment. The utilization of advanced diagnostic techniques allowed us to observe

specific indications of the material's degradation. As a result, once the exposure conditions are determined for accelerated aging, one can verify the lifetime of the nanomaterial-based product. The acquisition of complex data at certain periods of exposure provided an analysis of the aging progress of the film and determination of its application in specific conditions. The combined methodology was practically utilized to evaluate a new possible product line. Further research will be carried out to verify the most suitable product.

As presented here, AFM-based diagnostic methods provide a considerable amount of data to understand the degradation process of the tested film. In particular, the specific dimensions of the investigated object required the utilization of a high-sensitivity diagnostic tool, while both nanoparticles and film thickness would not be efficiently investigated using macroscale techniques.

Having such a complex experimental methodology, one can determine the market for this kind of test to be a few hundreds of thousands of dollars annually worldwide, and as nanomaterials become more popular, this market will grow exponentially. The obtained outcome confirmed the diagnostic readiness of the developed approach to be of interest to the industry (TRL 7–8). In fact, the next projects for both scientific and industrial applications were carried out recently. It should be underlined that one can implement it easily by utilizing the described protocol or its modified version tailored to the particular request of the end user. The main issue that requires implementation to enable common utilization of the probe technique in the assessment of the material's deterioration is the acquisition of sufficient data to correlate measurable changes in the surface's nanoscale properties with the product's usability limits and to standardize the AFM measurements to provide fully reliable and comparable data acquisition at each laboratory. Further industrial cooperation is recently desired, as it will provide the necessary data to continue the optimization of the presented diagnostic approach in terms of applications for various products and observation of a number of degradation processes. As a result, we expect the submicron measurements to be introduced in the market as a standard investigation tool in the abovementioned applications.

Supplementary Materials: The following supporting information can be downloaded at: https://www.mdpi.com/article/10.3390/app14083503/s1, Figure S1: roughness; Figure S2: Stiffness; Figure S3: Pull force; Figure S4: Wettability; Figure S5: Discoloration.

Author Contributions: Conceptualization, A.S.; methodology, A.S. and Ł.W.; investigation, A.S.; resources, Ł.W.; data curation, A.S.; writing—original draft preparation, A.S.; writing—review and editing, A.S.; visualization, A.S. All authors have read and agreed to the published version of the manuscript.

Institutional Review Board Statement: Not applicable.

Informed Consent Statement: Not applicable.

Data Availability Statement: The raw data supporting the conclusions of this article will be made available by the authors on request.

Conflicts of Interest: The authors declare no conflicts of interest.

References

1. Hospital Acquired Infections Infographic. Available online: http://chgbeds.blogspot.ca/2012/11/hospital-acquired-infections-infographic.html (accessed on 20 January 2024).
2. Ayobami, O.; Brinkwirth, S.; Eckmanns, T.; Markwart, R. Antibiotic Resistance in Hospital-Acquired ESKAPE-E Infections in Low- and Lower-Middle-Income Countries: A Systematic Review and Meta-Analysis. *Emerg. Microbes Infect.* **2022**, *11*, 443–451. [CrossRef] [PubMed]
3. Sevin, T.; Daniau, C.; Alfandari, S.; Piednoir, E.; Dumartin, C.; Blanchard, H.; Simon, L.; Berger-Carbonne, A.; Le Vu, S. Patterns of Antibiotic Use in Hospital-Acquired Infections. *J. Hosp. Infect.* **2021**, *114*, 104–110. [CrossRef] [PubMed]

4. Despotovic, A.; Milosevic, B.; Milosevic, I.; Mitrovic, N.; Cirkovic, A.; Jovanovic, S.; Stevanovic, G. Hospital-Acquired Infections in the Adult Intensive Care Unit—Epidemiology, Antimicrobial Resistance Patterns, and Risk Factors for Acquisition and Mortality. *Am. J. Infect. Control* **2020**, *48*, 1211–1215. [CrossRef] [PubMed]

5. Stewart, S.; Robertson, C.; Pan, J.; Kennedy, S.; Dancer, S.; Haahr, L.; Manoukian, S.; Mason, H.; Kavanagh, K.; Cook, B.; et al. Epidemiology of Healthcare-Associated Infection Reported from a Hospital-Wide Incidence Study: Considerations for Infection Prevention and Control Planning. *J. Hosp. Infect.* **2021**, *114*, 10–22. [CrossRef] [PubMed]

6. Mathur, P.; Malpiedi, P.; Walia, K.; Srikantiah, P.; Gupta, S.; Lohiya, A.; Chakrabarti, A.; Ray, P.; Biswal, M.; Taneja, N.; et al. Health-Care-Associated Bloodstream and Urinary Tract Infections in a Network of Hospitals in India: A Multicentre, Hospital-Based, Prospective Surveillance Study. *Lancet Glob. Health* **2022**, *10*, e1317–e1325. [CrossRef] [PubMed]

7. Chapa González, C.; González García, L.I.; Burciaga Jurado, L.G.; Carrillo Castillo, A. Bactericidal Activity of Silver Nanoparticles in Drug-Resistant Bacteria. *Braz. J. Microbiol.* **2023**, *54*, 691–701. [CrossRef] [PubMed]

8. Bruna, T.; Maldonado-Bravo, F.; Jara, P.; Caro, N. Silver Nanoparticles and Their Antibacterial Applications. *Int. J. Mol. Sci.* **2021**, *22*, 7202. [CrossRef] [PubMed]

9. More, P.R.; Pandit, S.; De Filippis, A.; Franci, G.; Mijakovic, I.; Galdiero, M. Silver Nanoparticles: Bactericidal and Mechanistic Approach against Drug Resistant Pathogens. *Microorganisms* **2023**, *11*, 369. [CrossRef] [PubMed]

10. Qiu, L.; Yang, H.H.; Lv, J.Y.; Fan, S.G.; Xie, M.H.; Wang, Z.J.; Gao, J.H. Study on the Bactriostasis of Nano-Silver against Four Strains of Bacteria. *Adv. Mater. Res.* **2014**, *1051*, 3–11. [CrossRef]

11. Kaiser, K.G.; Delattre, V.; Frost, V.J.; Buck, G.W.; Phu, J.V.; Fernandez, T.G.; Pavel, I.E. Nanosilver: An Old Antibacterial Agent with Great Promise in the Fight against Antibiotic Resistance. *Antibiotics* **2023**, *12*, 1264. [CrossRef] [PubMed]

12. Haji, S.H.; Ali, F.A.; Aka, S.T.H. Synergistic Antibacterial Activity of Silver Nanoparticles Biosynthesized by Carbapenem-Resistant Gram-Negative Bacilli. *Sci. Rep.* **2022**, *12*, 15254. [CrossRef] [PubMed]

13. Shahzadi, P.; Majeed, M.A.; Ibrahim, S.; Asif, S.; Kalsoom, R.; Hussain, I. Polymeric Coating Doped with Nanomaterials for Functional Impact on Different Substrates. *Sci. Rep.* **2024**, *14*, 578. [CrossRef] [PubMed]

14. *ISO 22196:2011*; Plastics–Measurement of Antibacterial Activity on Plastics Surfaces. Standard Webpage. Available online: https://www.iso.org/standard/54431.html (accessed on 11 April 2024).

15. *ISO 4892-2:2013*; Plastics—Methods of Exposure to Laboratory Light Sources—Part 2: Xenon-Arc Lamps. Standard Webpage. Available online: https://www.iso.org/standard/55481.html (accessed on 11 April 2024).

16. Rollet, F.; Morlat-Thérias, S.; Gardette, J.L. AFM analysis of CD-R photoageing. *Polym. Degrad. Stab.* **2009**, *94*, 877–885. [CrossRef]

17. Suresh, B.; Maruthamuthu, S.; Khare, A.; Palanisamy, N.; Muralidharan, V.S.; Ragunathan, R.; Kannan, M.; Pandiyaraj, K.N. Influence of thermal oxidation on surface and thermo-mechanical properties of polyethylene. *J. Polym. Res.* **2011**, *18*, 2175–2184. [CrossRef]

18. Yang, X.F.; Li, J.; Croll, S.G.; Tallman, D.E.; Bierwagen, G.P. Degradation of low gloss polyurethane aircraft coatings under UV and prohesion alternating exposures. *Polym. Degrad. Stab.* **2003**, *80*, 51–58. [CrossRef]

19. Sikora, A.; Bednarz, L.; Fałat, T.; Wałecki, M.; Adamowska, M. The investigation of the simulated solar radiation impact on the micro- and nanoscale morphology and mechanical properties of the sheet moulded composite surface. *Mater. Sci.* **2016**, *34*, 641–649. [CrossRef]

20. Wang, J.H.; Chang, C.-L.; Zhang, Z.W.; EL-Mahdy, A.F.M. Facile Metal-Free Synthesis of Pyrrolo[3,2-b]Pyrrolyl-Based Conjugated Microporous Polymers for High-Performance Photocatalytic Degradation of Organic Pollutants. *Polym. Chem.* **2022**, *13*, 5300–5308. [CrossRef]

21. Baumann, F.; Raga, S.R.; Lira-Cantú, M. Monitoring the Stability and Degradation Mechanisms of Perovskite Solar Cells by in Situ and Operando Characterization. *APL Energy* **2023**, *1*, 011501. [CrossRef]

22. Pinto, J.; Dias, M.; Amaral, J.; Ivanov, M.; Paixão, J.A.; Coimbra, M.A.; Ferreira, P.; Pereira, E.; Gonçalves, I. Influence of UV Degradation of Bioplastics on the Amplification of Mercury Bioavailability in Aquatic Environments. *Mar. Pollut. Bull.* **2022**, *180*, 113806. [CrossRef] [PubMed]

23. Sikora, A.; Grabarek, A.; Moroń, L.; Wałecki, M.; Kryla, P. The investigation of the light radiation caused polyethylene based materials deterioration by means of atomic force microscopy. *IOP Conf. Ser. Mater. Sci. Eng.* **2016**, *113*, 012016. [CrossRef]

24. Nowicki, M.; Richter, A.; Wolf, B.; Kaczmarek, H. Nanoscale mechanical properties of polymers irradiated by UV. *Polymer* **2003**, *44*, 6599–6606. [CrossRef]

25. Gryta, M.; Grzechulska-Damszel, J.; Markowska, A.; Karakulski, K. The influence of polypropylene degradation on the membrane wettability during membrane distillation. *J. Membr. Sci.* **2009**, *326*, 493–502. [CrossRef]

26. Kamińska, A.; Sawczak, M.; Ciepliński, M.; Śliwiński, G.; Kosmowski, B. Colorimetric study of the post-processing effect due to pulsed laser cleaning of paper. *Opt. Appl.* **2004**, *34*, 121–132.

27. Ekwińska, M.; Ekwiński, G.; Rymuza, Z. Calibration of normal force in atomic force microscope. In *Recent Advantages in Mechatronics*; Springer: Berlin/Heidelberg, Germany, 2007; pp. 505–510.

28. Ekwińska, M.; Rymuza, Z. Normal Force Calibration Method Used for Calibration of Atomic Force Microscope. *Acta Phys. Pol. A* **2009**, *116*, 78–81. [CrossRef]

29. Image Metrology Webpage. Available online: https://www.imagemet.com/ (accessed on 20 January 2024).

30. Czylkowski, D.; Hrycak, B.; Sikora, A.; Moczała-Dusanowska, M.; Dors, M.; Jasiński, M. Plasma surface modification of PMMA polymer and its composites with PCBM fullerene using an atmospheric pressure microwave argon plasma sheet. *Appl. Surf. Sci.* **2021**, *11*, 9270.

31. *ISO 19606:2017*; Fine Ceramics (Advanced Ceramics, Advanced Technical Ceramics) Test Method for Surface Roughness of Fine Ceramic Films by Atomic Force Microscopy. Standard Webpage. Available online: https://www.iso.org/standard/65457.html (accessed on 10 April 2024).

32. *ISO 23729:2022*; Surface Chemical Analysis Atomic Force Microscopy Guideline for Restoration Procedure for Atomic Force Microscopy Images Dilated by Finite Probe Size. Standard Webpage. Available online: https://www.iso.org/standard/79844.html (accessed on 10 April 2024).

33. Lochyński, P.; Sikora, A.; Szczygieł, B. Surface morphology and passive film composition after pickling and electropolishing. *Surf. Eng.* **2017**, *33*, 395–403. [CrossRef]

34. Ho, T.M.; Abik, F.; Mikkonen, K.S. An Overview of Nanoemulsion Characterization via Atomic Force Microscopy. *Crit. Rev. Food Sci. Nutr.* **2022**, *62*, 4908–4928. [CrossRef] [PubMed]

35. Ahn, B.; Jo, A.; Lee, J.; Cho, S.-J. Automatic Defect Review of a Patterned Wafer Using Hybrid Metrology. In Proceedings of the 2021 IEEE International Symposium on the Physical and Failure Analysis of Integrated Circuits (IPFA), Singapore, 15 September–15 October 2021; pp. 1–4.

36. *EN ISO/CIE 11664-4:2019*; Colorimetry Part 4: CIE 1976 L*a*b* Colour Space. Standard Webpage. Available online: https://www.iso.org/standard/74166.html (accessed on 11 April 2024).